



HAL
open science

Mapping of central africa forested wetlands using remote sensing

J. Betbeder, V. Gond, Frédéric Frappart, N. Baghdadi, G. Briant, E.
Bartholomes

► **To cite this version:**

J. Betbeder, V. Gond, Frédéric Frappart, N. Baghdadi, G. Briant, et al.. Mapping of central africa forested wetlands using remote sensing. *IEEE Journal of Selected Topics in Applied Earth Observations and Remote Sensing*, 2013, 7 (2), p. 531 - p. 542. 10.1109/JSTARS.2013.2269733 . hal-00966798

HAL Id: hal-00966798

<https://hal.science/hal-00966798v1>

Submitted on 28 Mar 2014

HAL is a multi-disciplinary open access archive for the deposit and dissemination of scientific research documents, whether they are published or not. The documents may come from teaching and research institutions in France or abroad, or from public or private research centers.

L'archive ouverte pluridisciplinaire **HAL**, est destinée au dépôt et à la diffusion de documents scientifiques de niveau recherche, publiés ou non, émanant des établissements d'enseignement et de recherche français ou étrangers, des laboratoires publics ou privés.

MAPPING OF CENTRAL AFRICA FORESTED WETLANDS USING REMOTE SENSING

BETBEDER¹ Julie; GOND¹ Valéry; FRAPPART² Frédéric; BAGHDADI³ Nicolas; BRIANT⁴ Gaël;
BARTHOLOME⁵ Etienne

- 1- CIRAD, Forest ecosystems goods and services, TA-C105, F-34398 Montpellier Cedex, (France)
- 2- Université de Toulouse; CNRS; IRD; OMP GET; 14 Avenue Edouard Belin, 31400 Toulouse, (France)
- 3- IRSTEA, UMR Tetis, 34196 Montpellier (France)
- 4- Département des sciences géomatiques, Pavillon L.-J.-Casault, Université Laval, Québec, G1K 7PK (Canada)
- 5- Joint Research Centre, European Commission, I-21027 Ispra (Italy)

Abstract

Wetlands represent 6% of the Earth's land cover surface. They are of crucial importance in the global water cycle and climatic dynamics. Nowadays, wetlands are the most threatened land cover type, nevertheless their spatial distribution and ecological functions are poorly documented. Despite the need for more detailed information, wetland mapping is a rarely activity. Few data are available mainly because of the complexity of obtaining good field data. We therefore propose a method based on multi sensor imagery analysis, to characterize land cover patterns of the second largest wetland area of the world (The 'Cuvette Centrale' of the Congo River basin). Time series of MODIS (Moderate Resolution Imaging Spectroradiometer) EVI (Enhanced Vegetation Index) images are used to map land cover types based their phenological differences. Flooded areas in the Congo Basin have been mapped during different seasons using L-band synthetic aperture radar (PALSAR) imagery. The associated model has been improved upon by the addition of elevation data as well as mean canopy heights acquired with LIDAR (Light Detection and Ranging) data. The result of this study is the first detailed spatial distribution of four forested wetland types within the 'Cuvette Centrale' of the Congo River basin. This study demonstrates that the spatial organization of the floodplain landscape depends on the extent of flooding. The results also show that land cover phenology is closely related to the time period of flood and solar intensity for this region, similarly to what is observed in the extensive floodplain of the Amazon basin.

Keywords: Remote sensing, large river floodplain forest, landscape, Congo River basin, PALSAR, MODIS, ICESat/GLAS

1. Introduction

Wetlands and floodplains, which cover approximately 6% of the Earth's ice-free land surface (Matthews & Fung, 1987; Organisation for Economic Cooperation and Development (OECD), 1996), have many economic uses and provide an abundance of ecological services (Frazier, 1999; Gosselink and Mitsch, 2000). Wetlands have a substantial impact on the alteration of flooding, flow rates, sediment stabilization, water quality, and groundwater recharge and discharge (Maltby, 1991; Bullock & Acreman, 2003). Wetlands also play a key role in biogeochemical cycles, including the methane (CH₄) and carbon dioxide (CO₂) cycles in particular (Matthews, 2000; Shindell *et al.*, 2004), and therefore exert influence on climate dynamics (RAMSAR convention, 1971). Wetlands are reservoirs of complex biological processes (Arfi, 2002), hot spots of biodiversity (Keddy *et al.*, 2009), and they are also crucial in the life cycle regulation of many fauna and flora species (Hey & Philippi, 1995). Wetlands also provide habitats for fishing and hunting and may contain wood suitable for harvesting or exploitation (Callicott & Frodeman, 2009). Despite the provision of multiple ecosystem services, wetlands appear to be the most threatened of all landscape types (Callicott & Frodeman, 2009). The threat to wetlands is testified by the loss of half of the world's wetlands during the last century. This decrease was mainly due to anthropogenic pressure and climate change (Mitsch & Gosselink, 2007; Murdoch *et al.*, 2000; Maltby, 1986). International and local institutions promoted the conservation of wetlands since the RAMSAR convention ratified in 1971. The emphasis on nature conservation increased over the last twenty years (Frazier, 1999; Convention for Biological Diversity, 1992).

Although many research efforts have attempted to characterize the large river floodplain of the Congo basin ecosystems so as to bolster their protection, the lack of knowledge regarding their spatial distribution and their ecological functions has hindered these efforts significantly (Junk &

1 Piedade, 2005). The forested wetlands within the 'Cuvette Centrale' of the Congo River basin, the
2 second largest basin in the world after the Amazon basin, are poorly documented. Various projects
3 at different levels of maturity proposed for example to transfer water from several tributaries of the
4 Congo River into lake Chad (Bonifica, 1982, 1984 and 1985; Misser, 2003; Turton & Ashton, 2004;
5 Biggs & Williams, 2001). These water transfers would produce substantial modifications to the
6 hydrological regime in the 'Cuvette Centrale' and hence would cause a significant threat to the
7 forested wetlands in the Congo River basin. The impacts of such a water transfer is also likely to be
8 amplified by climatic change within the region (IPCC, 2007). The risk of a degradation or even the
9 destruction of forested wetlands resulting from a significant reduction in high water levels due to
10 either natural or anthropogenic changes is particularly important. The lack of ecological as well as
11 hydrological information render corroborated decision making difficult.
12
13
14
15
16
17
18
19
20
21
22
23
24
25
26
27

28 In this respect, remote sensing (RS) offers a unique opportunity to map and describe landscape units
29 and forest types of areas where direct access is difficult. The spectral bands provided by RS sensors
30 allows the investigation of different aspects of these tropical swamp ecosystems. Optical data are
31 often used to characterize types of vegetation and deforestation (Vancustsem *et al.*, 2009; Peixoto *et*
32 *al.* 2009; Achard *et al.*, 2001; Wittmann *et al.*, 2002; Huete *et al.*, 2002), and these have also been
33 used in tropical areas even if dense cloud cover often makes characterization difficult. Radar RS
34 observations complement optical data because they provide valuable information even when
35 monitoring tropical land surfaces, which often have high cloud coverage. In addition, L-band SAR
36 sensors are very useful for the monitoring inundated wetlands (Rosenqvist *et al.*, 1999; Frappart *et*
37 *al.*, 2005). Light Detection and Ranging (LIDAR) has also been applied in remote areas for the
38 investigation of topography and maximum canopy height in flat areas (Lefsky *et al.*, 2007). In 2010,
39 Ballhorn *et al.* used ICESat/GLAS data (a space-borne LIDAR system) to estimate elevation and
40 canopy height in a peat-land region of Kalimantan, Borneo. Various estimates of forests biomass
41 were derived from these results.
42
43
44
45
46
47
48
49
50
51
52
53
54
55
56
57
58
59
60

1
2
3
4 The combination of information provided by both classes of sensors allowed us to study many
5 aspects of the tropical forest habitat, including not only its spatial distribution but also its structure
6 and certain ecological functions and processes. Two previous studies using RS data aimed to map
7 the wetland area within the 'Cuvette Centrale' of the Congo River basin. The first was conducted by
8 De Grandi *et al.* (1998) and used a single sensor approach and JERS-1 L-band SAR images to map
9 flooded and non-flooded forest areas. The second study, was conducted by Bwangoy *et al.* (2010)
10 using a multi-sensor approach, to produce a 'wetland probability map' for the 'Cuvette Centrale'
11 with a higher accuracy than the map created in the first study.
12
13
14
15
16
17
18
19
20
21
22
23

24 Though the forest types present in the 'Cuvette Centrale' have been well documented (Evrard,
25 1968), their spatial distributions have been poorly described due to difficulties of access to the
26 floodplain area, lack of infrastructure and political instability. Hence, the accurate mapping of the
27 spatial extension of the forest ecosystems within the 'Cuvette Centrale' is a strong requirement for
28 enabling the monitoring of land cover changes related to modifications in rainfall and the associated
29 hydrological regimes of the Congo River basin. Our objective is to document the spatial distribution
30 and functional description of the wetland land cover types, using a multi-imagery remote sensing
31 approach. This approach is fundamental for a continental water resources assessment for natural
32 and anthropogenic interpretation.
33
34
35
36
37
38
39
40
41
42
43
44
45

46 **2. Material and Methods**

47 ***2.1. Study area***

48
49
50 The Congo River basin harbors the second largest forest area in the world preceded only by the
51 Amazon River basin. The study area under consideration, the 'Cuvette Centrale', is located in the
52 center of the Congo River basin. It extends along the equator from 22° longitude west to 16°
53 longitude east and from 3° latitude north to 3° latitude south (Fig. 1). Bwangoy *et al.* (2010)
54
55
56
57
58
59
60

1 provided a map of this wetland area using a multi-sensor approach. From this study, a mask of the
2 forested wetland was used to delineate the area of the current study (Fig. 1).
3
4

5
6
7 [Figure 1]
8
9

10 11 12 *Physiography*

13 The ‘Cuvette Centrale’ is surrounded by mountains and plateaus and is the remnant of a lake that
14 occupied the area during the Tertiary geological period. It dried out as a consequence of the reduced
15 Congo downstream riverbed through the Crystal Mountains towards the Atlantic Ocean (Robert,
16 1946). Sandy, lacustrine quaternary sediments cover the base of the area where forested wetlands
17 are located (Lepersonne, 1974; Moukolo *et al.*, 1993; Censier, 1996). The topography is almost
18 without height differences, and the average slope is less than 7 cm/km between Kisangani and
19 Kinshasa (Devroey, 1957) over the last 50 km of the Kasai (Devroey, 1939) and over the last 450
20 km of the Ubangi downstream of Dongo (Yayer, 1951). Within the ‘Cuvette Centrale’, the Congo
21 River and its tributaries are bordered by discontinued levees that have been covered with flooded
22 forest (Yayer, 1951). The floodplain is not limited laterally by these levees, and floods can extend
23 over very large areas through networks of natural channels during high water seasons.
24
25
26
27
28
29
30
31
32
33
34
35
36
37
38
39
40
41

42 *Rainfall*

43 The average rainfall in the ‘Cuvette Centrale’ ranges between 1400 and 1800 mm. year⁻¹, with an
44 average of 1655 mm.year⁻¹ in Mbandaka (0.03 N, 18 E) (Fig. 2). Potential evapotranspiration is
45 1280 mm. year⁻¹ (FAO, 2000). More than 20% of the rainfall is available for runoff, as observed in
46 the discharge records in Brazzaville (Briquet, 1989; Shahin, 2002). Because of the topographic
47 barrier around the ‘Cuvette Centrale’, a large proportion of rainfall is believed to be of local origin;
48 it is thought to follow a closed cycle consisting of evaporated rainfall, condensation, and then again,
49 repeated rainfall (Robert, 1946).
50
51
52
53
54
55
56
57
58
59
60

1
2
3
4 [Figure 2]
5
6
7

8 *Hydrological regimes*
9

10 At the outlet of the 'Cuvette Centrale', only 6% of the discharge measured in Kinshasa and
11 Brazzaville originates from the upstream part of the Congo River basin, whereas 24% comes from
12 the 'Cuvette Centrale' itself. 23% comes from the Kasai River sub-basin, and less than 20% comes
13 from the Ubangi (Briquet 1993). In the 'Cuvette Centrale' between Kisangani and Mbandaka, the
14 flow rates of the Congo River are characterized by a bimodal flooding pattern, consisting of high
15 water in November and December, a secondary peak in April and May, low water in August and a
16 secondary minimum in February and March. In other words, there is a 1 to 2 month time lag
17 between flooding and rainfall seasonality (Fig. 2). Downstream of the Congo River, at Mbandaka,
18 water is received from its two main tributaries, the Oubangi and the Kasai Rivers. The Oubangi
19 extends its watershed over the two Congo tributaries and into the Central African Republic. The
20 Oubangi's flow rate is characterized by high waters reaching their maximum in November while
21 low water levels occur in March (Callède *et al.*, 2009). The Kasai is the main tributary of the Congo
22 River in the southern hemisphere. The watershed of the Kasai extends across the southern
23 hemisphere into the Democratic Republic of the Congo and Angola. The Kasai reaches the Congo
24 River at the downstream edge of the region where floodplain forest can be found. High water
25 regimes generally occur in April, while low water regimes occur during August, although there is a
26 small secondary high water period during December and January. In the downstream part of the
27 river basin, waters are higher in December than in April due to the influence of the Congo River.
28
29
30
31
32
33
34
35
36
37
38
39
40
41
42
43
44
45
46
47
48
49

50 Within the downstream portion of the river, the waters are higher in December than in April due to
51 the influence of the Congo's flow rate and the contribution of the Kasai tributaries that collect
52 waters from Lake Mai-Ndombe in the equatorial domain (Devroey, 1939). The typical flood
53 amplitude in the 'Cuvette Centrale' is between 3 and 5 m for the rivers (Devroey, 1957) and
54
55
56
57
58
59
60

1 approximately 2 m for the floodplain (Yayer, 1951). The volume of water that is potentially stored
 2 in the ‘Cuvette Centrale’ under the tree canopies can equals approximately half of the annual
 3 discharge from the Oubangi to the floodplain extending from the Congo River to the Likouala-aux-
 4 Herbes (Yayer,1951).
 5
 6
 7
 8
 9

10 *Vegetation*

11 The ‘Cuvette Centrale’ is primarily covered by forested wetland subjected to the flood pulse of the
 12 Congo River basin (Junk *et.al.*, 1989). The vegetation in this area is poorly studied (see Evrard
 13 (1968) for a review of the botanical inventories), as is the flood height and the flood length of each
 14 vegetation types. Indeed, the geographical conditions, the lack of infrastructure and the political
 15 instability make this area very difficult to access.
 16
 17
 18
 19
 20
 21
 22
 23
 24

25 Four forest types have been identified, but not spatially mapped in detail. The typology of the four
 26 forest types was establish taking into account Evrard’s inventories and the typology developed by
 27 Junk *et al.*, in 2011 for the Amazonian floodplain forest.
 28
 29
 30
 31

- 32 1) Forests subjected to relatively stable water levels (*Entandrophragma palustre*, *Coelocaryon*
 33 *botryoide* and *Raphiales spp.* palm forests);
 34
 35
- 36 2) Forests subjected to seasonal short lasting flood pulse of low amplitude (*Guibourtia*
 37 *deumeusei* and *Oubanguia africana*);
 38
 39
- 40 3) Non-flooded forests, characterized by higher and bigger trees (Evrard, 1968) and a more
 41 important diversity of tree species than the other groups and;
 42
 43
- 44 4) Forest subjected to seasonal flood pulse, located along the river (*Pachystela*
 45 *longepedicellata* and *Pseudospondias microcarpa*) (Léonard, 1947).
 46
 47
 48
 49

50 These forest types can be distinguished according to their stand structure and floristic composition.
 51
 52
 53
 54
 55
 56
 57
 58
 59
 60

2.2 mapping of forested wetlands by MODIS-Enhanced Vegetation Index (EVI)

EVI, a “16-Day L3 Global 500 m MODIS product (MOD13A1 c5)”, is a vegetation index. Data were acquired for the period from January 2001 till December 2009, and used to map the forested wetland types within the ‘Cuvette Centrale’ of the Congo River basin with respect to leaf phenology (Huete *et al.*, 2006). The values of EVI index have been derived from the multispectral measurements of the MODIS sensor onboard the NASA Terra satellite according to the following equation provided by Huete *et al.* (2002):

$$EVI = \frac{G \times (\rho_{NIR} - \rho_{RED})}{(\rho_{NIR} + C1 \times \rho_{RED} - C2 \times \rho_{BLUE} + L)}$$

(Eq. 1)

Where ρ_{NIR} [841–876 nm], ρ_{RED} [620–670 nm] and ρ_{BLUE} [459–479 nm] are the reflectances of near infrared, red and blue bands respectively, G is the gain factor, L is the canopy background adjustment (that addresses non-linear, differential NIR and red radiant transfer through a canopy) and C1, C2 are the coefficients of the aerosol resistance terms (which use the blue band to correct aerosol influences in the red band). The coefficients used in the MODIS-EVI algorithm are: L=1, C1 = 6, C2 = 7.5, and G (gain factor) = 2.5. This dataset is available at <http://reverb.echo.nasa.gov>.

The EVI value is considered to be closely related to canopy structure and architecture. The EVI also provides improved sensitivity compared with other vegetation indices for high biomass regions, such as the tropical forest (Myneni *et al.*, 2007; Huete *et al.*, 2002).

To reduce atmospheric bias and remaining ‘contaminated’ pixels after classical atmospheric corrections (see Huete *et al.*, 2002), time-composited EVI imagery (2000-2009) has been used. According to Pennec *et al.* (2010), an average for each 16-day period is calculated over the ten-year time span examined in this study.

An unsupervised k-means classification is then performed for yearly averaged EVI imagery. To determine the optimal number of land cover classes, we used the Thorndike index (Thorndike *et al.*, 1953):

$$S_k = \frac{1}{N} * \sum_{k=1}^{k_{\max}} n_k * \sum_{k=1}^{k_{\max}} \sum_{i=1}^{i_{\max}} \sigma_{ik}^2$$

(Eq. 2)

Here, N represents the total number of pixels, n_k is the number of pixels by class, k is the class index varying between 1 and k_{\max} , i is the index of the 16-day period (from 1 to $i_{\max}=23$), and σ_{ik}^2 is the variance of the class k for the period i . The optimum number of classes is obtained using the classes that correspond to the inflection point of the S_k index.

Aerial photographs (IGN, 1961) of the Northern part of the Democratic Republic of the Congo and a topographic map of the same Northern part (IGN - Institut Géographique National 1960) with forested wetland types mapped were used to validate the EVI data. The aerial photographs represent 15 000 km² of the ‘Cuvette Centrale’; their references are AE-1960-61-NA33XI-XII (from 0 to 532) and AE-1961-62-NA33V-VI (from 248 to 524).

A comparison was established between two areas of the ‘Cuvette Centrale’, respectively the Eala and Lukulela areas, regarding the phenology of the EVI index and ancillary data (Fig .1). The ancillary data include rainfall (mm), light intensity (cal g/cm²/day) (Evrard, 1968) and the hydrology of the nearest river recorded with gauging data (Devroey, 1957; Bultot, 1971; Laraque & Maziézoula, 1995).

2.3 Estimation of tree heights using GLAS/ICESat L2 Global Land Surface Altimetry data

The Geoscience Laser Altimeter System (GLAS) instrument of the Ice, Cloud, and Land Elevation Satellite (ICESat) is a full waveform sensor consisting of a 1.064 μm laser at 40 Hz that has been operational from 2003 to 2010. The GLAS sensor acquired the returned energy of a footprint of 0.70 m and creates a waveform enabling the measurement of terrain elevation and the vertical distribution of vegetation density. This dataset includes laser footprint geo-location and reflectance as well as geodetic, instrumental, and atmospheric corrections for the range measurements. The dataset is available at <http://reverb.echo.nasa.gov>.

The LIDAR technique has been used to detect the topography (Blair & Hofton, 1999) of the “footprint” and to estimate the maximum height of the canopy for each forest type. Waveform analysis enables one to approximate the maximum height of the canopy for flat terrain (Lefsky *et al.*, 2007; Neuenschwander *et al.*, 2008) as well as topographical elevation (Ballhorn, *et al.*, 2010). The interpretation of these data is more complex for an area with a slope, where vegetation and ground reflectance are mixed in the signal return (Chen, 2010).

Two kinds of products have been used to study the waveform:

- 1) GLA01 as the raw product;
- 2) GLA14 which provides an approximation of beginning and end signals by fitting the complex waveform from GLA 1 into six Gaussian maximum peak distributions (Zwally *et al.*, 2003; Harding & Carabajal, 2005).

From these Gaussian peaks, vegetation structure and topography could be extracted. All ICESat/GLAS data available for the ‘Cuvette Centrale’ from February 2003 to January 2009 were procured. The GLA14 data available were converted into shape vector files to enable overlays with EVI based classifications and ICESat tracks. This makes it possible to select corresponding MODIS footprints.

Two hundred footprints (issued from the unsupervised classification of MODIS data) were selected by EVI class to analyze the correlation between topography and spatial distribution for the different types of forested wetlands. The maximum height of the forested wetland types was determined by waveform analysis using the distance between the beginning of the signal and the centroid of the ground return (Ballhorn *et al.* 2010).

2.4 Estimating inundation by ALOS PALSAR

The Phased Array type L-band Synthetic Aperture Radar (PALSAR) sensors on board of the L-band Advanced Land Observing Satellite (ALOS) have been chosen to study the process of inundation. Six images, which were acquired on 1/25/2009, 3/15/2010, 4/27/2009, 09/07/2007, 10/25/2008, and 12/13/2009, have a horizontal/horizontal polarization and a 100 m spatial resolution at various viewing angles (from 18° to 43°).

SAR imagery is sensitive to the presence of water located under the vegetation canopy since the backscattered signal is significantly increased due to the radar double-bounce returns from the water and vegetation surfaces. The ScanSAR imagery has been pre-processed with respect to radiometric calibration, incidence angle normalization and speckle reduction. The imagery has first converted into sigma nought (σ_0) in dB (ALOS PALSAR, 2008). The angle of incidence effect on the backscattering coefficients have been corrected using the procedure developed by Baghdadi *et al.* (2001). The normalized backscattering coefficient is given by:

$$\sigma_n^\circ = \frac{\sigma^\circ(\theta_i)}{F(\theta_i)} \quad (\text{Eq. 3})$$

Here, $\sigma^\circ(\theta_i)$ represents the backscattering coefficient (dB) at the incidence angle θ_i .

In linear units, $\sigma^\circ(\theta_i)$ is given by the relation $\beta \cos^\alpha \theta$ (Ulaby *et al.*, 1982; Beauchemin *et al.*, 1995). Thus, $F(\theta)$ is of the form $\beta \cos^\alpha \theta$, and the normalized backscattering coefficient (β) is given

1
2 as $\sigma^\circ(\theta_i) / \cos^\alpha \theta_i$ (Baghdadi *et al.*, 2001). For each date of acquisition, the coefficient α is equal to
3
4 the slope of the linear relationship between σ° (dB) and $10 \log [\cos(\theta)]$, which has been
5
6 established using ten homogeneous regions of interest (ROI's) chosen in the non-flooded forest and
7
8 at an incidence angle between 18° and 43° . A Lee filter (Zhenghao & Fung, 1994) has subsequently
9
10 been applied to a window of 7×7 pixels to reduce speckle. Similar to EVI, an unsupervised k-means
11
12 classification was performed for an optimum number of classes. This unsupervised classification
13
14 was applied to a temporal series of PALSAR scenes, which represented different periods of flooding
15
16 in the study area. To study the dynamics of inundation, each class was averaged.
17
18
19
20
21

22 A χ^2 -test was used to establish the relationship between an EVI class and a PALSAR class.
23
24
25
26

27 3. Results

31 3.1 EVI classification for forested wetland types

32
33
34
35 Based on the Thornlike index presented in Fig. 3, the optimum number of EVI-based forest classes
36
37 has been determined using the elbow effect (Tibshirani *et al.*, 2001). An unsupervised classification
38
39 for the EVI average year was performed, and the results were clustered into four classes (Fig. 3).
40
41
42
43

44 [Figure 3]
45
46
47
48

49 The classification result is shown in Fig. 4. The class EVI-1 of forest is located mainly alongside
50
51 rivers and large lakes. This class is also present in the southwestern part of the Congo River basin
52
53 and northwest of Lake Tele. EVI-1 covers an area of 24 000 km². The EVI-2 class is present in the
54
55 central region of the 'Cuvette Centrale' and covers 85 000 km². The EVI-3 class covers 121 000
56
57 km² and is frequently associated with the EVI-2 class. The EVI-4 class covers a smaller area (56
58
59
60

1
2 000 km²) and occurs near Lake Tele in the north of the 'Cuvette Centrale' along the Oubangui River
3
4 as well as in the south near the lakes and tributaries of the Congo River.
5
6
7

8 [Figure 4]
9
10

11
12 The EVI classification has been compared and validated using two different datasets: the
13 topographic map of Northern Congo (IGN, 1960) and the soil and tree elevations derived from the
14 GLAS measurements. Thematic accuracy of the EVI vegetation map was assessed using a χ^2 test
15 and a contingency table according to the IGN topographic map and the spatial distributions of the
16 EVI classes. These results are shown in Fig. 5. EVI class footprints and transitions between EVI
17 classes have been visually photo-interpreted using aerial photographs (shape, location and map).
18
19
20
21
22
23
24
25
26
27

28 [Figure 5]
29
30
31
32

33 GLAS data allow for the acquisition of average elevations and maximum canopy heights for three
34 EVI classes (Table 1). Class EVI-1 does not produce results due to the lack of ICESat-GLAS data
35 for this type of forest. At least one EVI class elicits elevations significantly different from the others
36 (ANOVA, p-value < 0.5). On average, the EVI-2 class is associated with the lowest elevations and is
37 characterized by the lowest maximum canopy height. On average, the elevation of the EVI-4 class
38 is higher than that of the other classes and demonstrates the largest maximum canopy height.
39
40
41
42
43
44
45
46
47

48 [Table 1]
49
50
51
52

53 Time series analysis suggests that differences between EVI classes are not linked with phenological
54 patterns (Fig. 6). Although the EVI classes demonstrate a similar temporal evolution, they display
55 different magnitudes of EVI values. Each forested wetland type is characterized by a leaf phenology
56
57
58
59
60

1 cycle with two peaks of activity during May and October separated by a decrease of leaf density in
2
3
4 December and August. Each EVI class exhibits similar characteristics, and an EVI mean value
5
6 increasing as the class type changes from EVI-1 to EVI-4 (Fig. 6). These variations are mostly
7
8 based on the intensity of the greenness related to the EVI index.
9

10 [Figure 6]
11
12
13

14 **3.2 PALSAR-derived inundation classification**

15
16
17
18
19 The optimum number of classes has been determined using the Thornlike index. For the series of
20
21 PALSAR images of the 'Cuvette Centrale', the optimum number of classes is five (Fig. 7). One
22
23 class represents the borders of the image, and its value is equal to zero for each of the PALSAR
24
25 images examined.
26
27

28
29
30 [Figure 7]
31
32
33
34

35 The time variations of the backscattering coefficients for each class are shown in Fig. 8. Four areas
36
37 with distinct flooding patterns can be observed. The temporal dynamics of the backscattering
38
39 coefficients for each class allow the characterization of each class in terms of inundation and land
40
41 cover. PALSAR-1 data reveal low backscatter values associated with large annual amplitude that
42
43 peaks in March/April at approximately -12.5 dB and reaches a minimum of -18 dB in October.
44
45 PALSAR-2 data have an almost constant backscatter coefficient with values between 7.5 to 8.5 dB,
46
47 regardless of the season. PALSAR-3 data elicit the highest backscatter values, between 4.5 and 3.5
48
49 dB. The maximum is observed at the end of the year. PALSAR-3 data have a temporal evolution
50
51 close to that of PALSAR-2 between December and April and close to PALSAR-4 data between May
52
53 and October.
54
55

56
57 [Figure 8]
58
59
60

1
2
3
4 Fig. 9 presents the spatial distribution of the flooding area's derived from an unsupervised
5 classification of PALSAR imagery. The PALSAR-1 class is typically located outside the 'Cuvette
6 Centrale' and along the Oubangui River. The PALSAR-2 class is observed along the large rivers,
7 such as the Congo River itself, and within the western portion of the 'Cuvette Centrale'. The
8 PALSAR-3 class is located in the center and west of the Cuvette Centrale. The PALSAR-4 class is
9 typically located in the vicinity of the PALSAR-3 class.
10
11
12
13
14
15
16
17
18
19

20 [Figure 9]
21
22
23
24
25

26 3.3 Classification comparisons 27 28 29

30 The two classifications presented above exhibit strong dependency (χ^2 test, p -value < 0.005). Thus,
31 these results are combined to analyze the nature of the landscape (EVI classes) in relation to
32 flooding status (PALSAR classes).
33
34
35
36
37
38

39 [Figure 10]
40
41
42
43
44
45

46 4. Discussion 47 48 49

50 The results of this study are the first to describe the spatial distribution of the forested wetland types
51 in the 'Cuvette Centrale' of the Congo Basin, in detail. The multi-sensor approach applied, produces
52 a better understanding of the phenology, the structure and the flooding periods of the different forest
53 types.
54
55
56
57
58
59
60

4.1 Spatial distribution of the forested wetland

The complementary use of three data sources permitted the classification of the different forested wetland types. The four forested wetland types identified by Evrard in 1968 were discriminated and mapped based on their leaf phenology using EVI imagery data. Each of these four forested wetland types have different greenness intensities but the same seasonality. Thus, our hypothesis is that the discrimination of forested wetland types according to the EVI index is based on the stand structure of each type. The density of the cover has also been shown to be significant, and the EVI index value was shown to be high (Huete *et al.*, 2006). The structure is clearly identified on the stereo aerial photography and is related to the intensity of the EVI index (Pennec *et al.*, 2011). Class EVI-2 consists of sparse stands of forest canopy, whereas class EVI-4 has a closed stand forest structure composed of different understory strata. In general, a forest type with a multi-layered stratified canopy and a closed crown cover generates a greater EVI signal than a single-layered canopy with an open crown cover (Gond *et al.*, 2011).

The map obtained for this study offers a good spatial and thematic accuracy compared to the IGN topography map from 1960. Moreover, the vegetation exhibits a marked zonation related to the flooding regime (relationship with PALSAR dataset) as the floodplain vegetation of the Amazon and Okavango basins (Parolin *et al.*, 2010). The GLAS data permit the evaluation of the average elevation and the maximum canopy height for three forested wetlands, which is in agreement with the Evrard and Leonard (1947) indications for emergent trees of seasonal flooded forest. However we notice that it is possible that GLAS data overestimate the maximum canopy height because in the Amazon floodplain, the forests subjected to relatively stable water level reaches an average height of 15-20 meters (Scarano *et al.*, 1997).

4.2 Hydrological dynamics

Four hydrological dynamics were identified using the PALSAR multi-temporal images that can be related to the vegetation map.

In general, radar backscattering is lower for an open water body than for other surfaces. This is due to specular reflection from the water surface. This is a characteristic which permits the accurate determination of the extent of the flooding area for open water bodies, such as rivers and lakes not covered with vegetation. Moreover, the L-band has extensive higher canopy penetration depth, permitting the detection of water surfaces below the canopy. The multi-temporal use of L-band imagery allows the discrimination between forest subjected to relatively stable water level, forest subjected to seasonal flood pulse and non-flooded areas. As shown in Fig. 8, there is no overlap of the mean values with their standard deviations indicated, for each class. The PALSAR imagery in the ScanSAR mode allows us to detect flooding over large areas (*i.e.*, from 250 to 350 km, or three to five times the footprint of a conventional SAR scene).

Regarding PALSAR image classification, the PALSAR-1 class elicits the lowest level of backscattering and can be used to identify non-covered water surfaces (rivers and lakes). Increasing backscattering coefficients during the low water season (March/April) are likely to be the consequence of the presence of islands and vegetation species found in the river channels and the open water of the Likouala-aux-Herbes and Moanda Rivers. PALSAR-2 exhibits very low backscatter variation over a year and a relatively low mean backscattering value. This is assumed to be originating from volume as well as multiple scattering mechanisms of non-flooded forests (Martinez & Le Toan, 2007; Evans *et al.*, 2010). PALSAR-3 has the highest backscattering coefficient values due to the double-bounce effect of the interactions of the radar pulse with

1 vegetation trunks and the underlying water surface (Hess *et al.*, 1995; Wang *et al.*, 1995). Because
2 the backscattering coefficient has low temporal dynamics (less than 1.5 dB), this signature can be
3 attributed to the forest subjected to relatively stable water levels. PALSAR-4 exhibits time
4 variations similar to those of PALSAR-2 (non-flooded forests) during low water level periods
5 (March/April) and variations similar to those of PALSAR-3 (forest subjected to relatively stable
6 water level) during high water level periods (October/January). This class is associated with forests
7 subjected to seasonal short lasting flood pulse, with low amplitude (<5m, Yayer, 1951). At the end
8 of the year, the PALSAR-4 backscatter is lower than the PALSAR-3 return, which is likely to be
9 due to the tree density of forests subjected to seasonal flood pulse compared to the low density of
10 forests with stable water level.
11
12
13
14
15
16
17
18
19
20
21
22

23 The results of this study have been partially validated using the Congo River and Oubangui water
24 levels in the 'Cuvette Centrale'. These water levels represent the increased water levels at the end of
25 the year (November-December) and the lower water levels in March and April from the PALSAR-4
26 profile (Fig. 8). In terms of the dynamics and backscattering values, these results are consistent with
27 those recently published for forest units, including flooded and non-flooded forests, using ALOS
28 PALSAR data for the classification of different types of tropical and temperate forests (Thiel *et al.*,
29 2009; Ardila, *et al.*, 2010; Evans *et al.*, 2010).
30
31
32
33
34
35
36
37
38
39
40
41
42
43

44 The comparison of the EVI and PALSAR classifications with the IGN topographic map
45 demonstrates agreement for the spatial units obtained. However, we must consider that the 'Cuvette
46 Centrale' of the Congo River basin is located on the equator and is therefore located in both the
47 southern and the northern hemispheres, which each have distinct hydrologic systems (Devroey,
48 1957). The PALSAR ScanSAR dataset currently available for this area only allows us to consider
49 two seasons, the beginning and the end of the year. As a result, neither specific months nor the
50 contribution of each tributary of the 'Cuvette Centrale' to the global inundation has been studied in
51
52
53
54
55
56
57
58
59
60

1 detail. Detailed monitoring of inter-annual variation regarding the extent of flooding within this
2
3
4 vegetation landscape is not currently accessible with ALOS radar data.
5
6
7

8 4.3 Classifications comparisons 9

10
11
12 We find similar forested wetland types using both approaches (PALSAR and EVI mapping (χ^2
13 test)). The spatial distribution of the EVI classes is driven by flooding status (stable water level,
14
15 seasonal flood pulse, and no flooding). The EVI-4 class corresponds to the “no flooding” PALSAR
16
17 class. Since this region is labeled on the topographic map as *non-flooded* forest, this is consistent
18
19 with our results.
20
21
22
23

24
25
26 Given the relationship between EVI, GLAS, and PALSAR data and based on published data, we
27
28 propose the following labels for EVI classes (Fig. 4):
29

- 30 - EVI-1 consists of forest subjected to seasonal flood pulse, located alongside rivers, as
31 described by Evrard (1968)
32
- 33 - EVI-2 consists of forests subjected to stable water level, dominated by *Raphiales*, occurring
34 at an average elevation of 304 m, and with a 20 m maximal canopy height;
35
36
- 37 - EVI-3 consists of forests subjected to seasonal short lasting flood pulse, with low amplitude,
38 as described by Evrard (1968), located at an average elevation of 306 m and with a 30 m
39 maximum canopy height;
40
41
- 42 - EVI-4 consists of non-flooded forests located at an average elevation of 311 m and with a 40
43 m maximum canopy height.
44
45

46 To illustrate these classes, we show four field photographs (Fig. 10).
47
48
49
50
51
52
53
54
55
56
57
58
59
60

4.4 Vegetation dynamics

The current study demonstrates also that in the ‘Cuvette Centrale’ of the Congo River basin, there is a strong relationship between high photosynthetic activity (EVI), a high level of light intensity (Evrard, 1968), a low level of flooding and a high level of rainfall. The forested wetlands of the Congo River ‘Cuvette’ loop through four phenological phases (two rainy and two dry seasons; Fig. 11). Without the contribution of any field measurements, we hypothesize that some species may shed their leaves during the flooding periods (December to January and July to August), as the Amazonian floodplain trees (Schöngart *et al.*, 2002; Haugaasen & Perez, 2005).

[Figure 11]

At the beginning of the year (February to March), the water level of the Congo River is at its minimum, and the light intensity and rainfall increase (Devroey, 1957). The EVI demonstrates a similar increase likely corresponding with the growth of the vegetation. Rainfall and light intensity are relatively stable from March to May when Congo River flooding typically occurs (maximally in May). Then, the EVI index values increase until May, when they reach the first peak of activity, and then decrease until July. Each of the other variables also decreases until the minimum light intensities occurs in July that causes consequent photosynthetic activity decrease. This period also corresponds to large rainfall causing floods in the Congo.

Beginning in August and reaching a maximum in October, there are simultaneous increases in light intensity and photosynthetic activity, rainfall, Congo and Oubangui River floods. Additionally, these parameters reach secondary peaks of activity in October.

At the end of the year, light intensity, photosynthetic activity and rainfall decrease between November and January, which is concurrent with the maximum level of the Congo River flooding (December) and the high level of the Oubangui River. This period is also marked by lower

1 greenness activity.
2
3
4
5

6 Previous studies (Parolin *et al.*, 2010; Schöngart, *et al.*, 2002) have shown that the phenology of
7 seasonal flooded forest (*e.g.*, in várzea and igapó) is dependent on the maximum level of
8 inundation. However, the phenology of *terra firma* forest in the Amazon Basin was shown to be
9 driven by rainfall as well as light intensity (Haugaasen & Peres, 2005). Flooded and non-flooded
10 forests react in a similar way; the main drivers of phenology are light and rainfall for non-flooded
11 forest, and flooding and light intensity for flooded forests. Indeed, light intensity plays a key role. It
12 is possible that light intensity could influence the two peaks of photosynthetic activity for each
13 forest type because low levels of light intensity and a hydric stress occur during dry periods
14 (Farnsworth *et al.*, 2011; Camberlin *et al.*, 2001). Most likely many environmental parameters play
15 key roles in the phenology of intrinsic factors related to the phylogenetic origin of the species or
16 genus (Wright & van Shaik, 1994).
17
18
19
20
21
22
23
24
25
26
27
28
29
30
31
32

33 **5. Conclusion**

34
35
36
37 This paper explores the use of a multi-sensor approach for the thematic characterization of forested
38 wetland types within the Congo River basin and demonstrates that each type of sensor provides
39 complementary information for the investigation of the spatial distribution, inundation and leaf
40 phenology of forested wetland types.
41
42
43
44

45
46 The unique feature of the ‘Cuvette Centrale’, compared to Amazonia, is that the rainy season occurs
47 twice per year (April-May and September-October). The spatial distribution of forested wetland
48 types is controlled by topography and also by the time and the intensity of the submersion. Any
49 changes in this parameter can modify the organization and the functioning of the forested wetlands.
50
51 The phenology of forested wetlands is already modified from year to year according to the inter-
52 annual variations of eco-climatic parameters.
53
54
55
56
57
58
59
60

1 This study investigates a new area of research regarding the ‘Cuvette Centrale’ floodplain in the
2 Congo River basin. With the spatial distribution and the brief functional description provided, it is
3 now possible to investigate this large ecosystem with more details. The documentation and the
4 study of this huge remote area are fundamental for understanding continental natural resources
5 involved in freshwater regulation, carbon stocks and basic chemical element exchanges at the
6 tropical atmosphere-biosphere interface.
7
8
9
10
11
12
13
14
15
16

17 **Acknowledgments**

18 The authors thank NASA, ESA and IRD for providing the remote sensing data. This study was
19 supported by CIRAD funding. The authors also thank Frederique Seyler, Sylvie Gourley-Fleury,
20 and Yves Laumonier for their help.
21
22
23
24
25
26
27
28
29
30
31
32
33
34
35
36
37
38
39
40
41
42
43
44
45
46
47
48
49
50
51
52
53
54
55
56
57
58
59
60

References

ALOS/PALSAR (2008). Level 1 product. Format description. Level 1.1/1.5, JAXA Earth Observation Research Center, Harumi, Japan.

Ardila, J.P., Tolpekin, V., Bijker, W. (2010). Angular backscatter variation in L-band ALOS ScanSAR images of tropical forest areas, *IEEE Geoscience and Remote Sensing Letters*, 7 (21), 821-825.

Arfi R. (2002). Processus d'édification des ressources naturelles en zones inondables tropicales. In : Orange Didier (ed.), Arfi Robert (ed.), Kuper M. (ed.), Morand Pierre (ed.), Poncet Yveline (ed.), Témé B. (préf.) Gestion intégrée des ressources naturelles en zones inondables tropicales. Paris (FRA) ; Bamako : IRD ; CNRST, p. 169-178. (Colloques et Séminaires). GIRN-ZIT : Gestion Intégrée des Ressources Naturelles en Zones Inondables Tropicales : Séminaire International, Bamako (MLI), 2000/06/20-23. ISBN 2-7099-1480-8.

Baghdadi, N., Bernier, M., Gauthier, R., & Neeson, I. (2001). Evaluation of C-band Sar data for wetlands mapping. *International Journal of remote sensing*, 22(1), 71-88.

Beauchemin, M., Thomson, K., & Edwaeds, G. (1995). Modelling forest stands with MIMICS: implications for calibration. *Canadian Journal of Remote Sensing*, 21, 518-526.

Biggs D. & Williuams R. (2001). A case study of integrated water resource management in windhoek, Namibia. Proceedings of symposium “frontiers in urban water management: deadlock or hope?”, Marseille 18-20 June 2001 Workshop 1: demand management practice, policy, data and technologies. IHP-V Technical documents in hydrology n° 45, UNESCO – Paris, p 10-18.

Blair, J.B., & Hofton, M.A. (1999). Modeling laser altimeter return waveforms over complex vegetation using high-resolution elevation data. *Geophysical Research Letters*, 26, 2509-2512.

Bonifica, (1982), (1984) and (1985): Transaqua. Bonifica S.p. A. I.R.I ITALSAT, Roma.

Briquet, J.-P. (1989). Proceedings of “Quatrièmes journées hydrologiques de l'ORSTOM à Montpellier 14-15 Sept. 1988. ORSTOM Paris – collection “Colloques et séminaires”, p 131-146.

1 **Briquet, J.-P.** (1993). Les écoulements du Congo à Brazzaville et la spatialisation des apports.
2
3 Proceedings from the conference “Grands bassins fluviaux périatlantiques: Congo, Niger,
4
5 Amazoné” (INSU-CNRS-ORSTOM), Paris 22-24 Nov 1993, p 27-38.
6
7

8 **Bullock, A. & Acreman, M.** (2003). The role of wetlands in the hydrological cycle. *Hydrology and*
9
10 *Earth System Sciences*, 7(3): 358-389.
11

12 **Bwangoy, J-R. B., Hansen, M. C., Roy, D. P., De Grandi, G., & Justice, C.O.** (2010). Wetland
13
14 mapping in the Congo Basin using optical and radar remotely sensed data and derived topographical
15
16 indices. *Remote Sensing of Environment*, 114, 73-86.
17

18 **Callède J., Boulvert Y., & Thiebaut J.-P.** (2009). Le bassin de l'Oubangui. Coll. Monographies
19
20 hydrologiques, ORSTOM Paris (CD ROM).
21
22

23 **Censier C.** (1996). Caractérisation de processus d'érosion régressive par analyse sédimentologique
24
25 comparée des sables du chenal et des barres du cours inférieur de l'Oubangui (République
26
27 Centrafricaine, Congo, Zaïre). Proceedings of conference “L'hydrologie tropicale: géoscience et
28
29 outil pour le développement”, Paris May 1995. IAHS Publication. 238, 1996 p 289-303
30
31

32 **Chen, Q.** (2010). Retrieving vegetation height of forests and woodlands over mountainous areas in
33
34 the Pacific Coast region using satellite laser altimetry. *Remote Sensing of Environment*, 114, 1610-
35
36 1627.
37
38

39 **De Grandi, G.-F., Rosenqvist, A., Mayaux, P., Rauste, Y., Kattenborn, G., Simard, M.,**
40
41 **Saatchi, S. & Leysen, M.** (1998). Flooded Forest Mapping at Regional Scale In the Central Africa
42
43 Congo River Basin: First Thematic Results Derived by ERS-1 and JERS-1 Radar Mosaics, Second
44
45 Retrieval of Bio- and Geo-physical Parameters from SAR data for Land Applications, October
46
47 1998, ESTEC, The Netherlands.
48
49

50 **Devroey E.-J.** (1939). Le Kasai et son bassin hydrographique. Annales des Travaux Publics de
51
52 Belgique, Bruxelles, 334 pages.
53
54

55 **Devroey E.-J.** (1957) Annuaire hydrologique du Congo belge et du Ruanda – Urundi 1956.
56
57 Académie Royale des Sciences Coloniales. Bruxelles, Classe Sciences et Techniques. Memoires. in-
58
59
60

1
2
3
4
5
6
7
8
9
10
11
12
13
14
15
16
17
18
19
20
21
22
23
24
25
26
27
28
29
30
31
32
33
34
35
36
37
38
39
40
41
42
43
44
45
46
47
48
49
50
51
52
53
54
55
56
57
58
59
60

8°, nouvelle Série T. VII Fasc. 3 469 pages.

Evans, T.L., Costa, M., Telmer, K., & Silva, T.S.F. (2010). Using ALOS/PALSAR and RADARSAT-2 to Map Land Cover and Seasonal Inundation in the Brazilian Pantanal, *IEEE Journal of Selected Topics in Applied Earth Observations and Remote Sensing*, 3(4), 560-575.

Evrard, C. (1968). Recherches écologiques sur le peuplement forestier des sols hydromorphes de la Cuvette Congolaise Centrale. Bruxelles, Des presses des Ets WELLENS-PAY s.a, 1968, 295 p.

FAO (2000). FAOCLIM 2: worldwide agroclimatic database. FAO Agrometeorology Group, Rome, CD ROM.

Farnsworth, A., White, E., Williams, C., Black, E., Kniveton, R. (2011). Understanding the large scale driving mechanisms of rainfall variability over Central Africa, in C.J.R., Williams, D.R. Kniveton (eds.), African Climate and Climate Change, Advances in Global Change Research 43, Doi 10.1007/978-90-481-3842-5_5, Springer Science+Business Media B.V. 2011.

Frappart, F., Martinez, J. M., Seyler, F., León, J. G. & Cazenave, A. (2005). Floodplain water storage in the Negro River basin estimated from microwave remote sensing of inundation area and water levels *Remote Sensing of Environment*, 99(4), 387-399.

Frazier, S. (1999). Ramsar Sites Overview. A Synopsis of the World's Wetlands of International Importance. *Wetlands International*. 58 pp.

Gond, V., Freycon, V., Molino, J.-F., Brunaux, O., Ingrassia, F., Joubert, P., Pekel, J.-F., Prévost, M.F., Thierron, V., Trombe, P.-J., Sabatier, D. (2011). Broad scale patterns of forest landscape in Guiana Shield rain forests, *International journal of Applied Earth Observation and Geoinformations*, 13, 357-367. Doi: 10.1016/j.jag.2011.01.004

Haugaasen, T. & Peres, C. A. (2005) Tree phenology in adjacent Amazonian flooded and unflooded forests. *Biotropica*, 37(4), 620-630.

1
2 **Hess, L. L., Melack, J. M., Filoso, S. & Wang, Y.** (1995). Delineation of inundated area and
3
4 vegetation along the Amazon floodplain with SIR-C synthetic aperture radar. *IEEE Trans. Geosci.*
5
6 *Remote Sensing*, 33, 896-904.

7
8 **Hey, D. L. & Philippi, N. S.** (1995). Flood reduction through wetland restoration: the upper
9
10 Mississippi river basin as a case history. *Restoration Ecology*, 3(1), 4-17.

11
12 **Hladik, A.** (1978). Phenology of leaf production in rain forest of Gabon: distribution and
13
14 composition of food for folivores. Page 41-72 in Montgomery G. ed. The ecology of arboreal
15
16 folivores. Smithsonian Institution Press. Washington, D. C.

17
18 **Huete, A.R., Didan, K., Miura, T.R.E.P., Gao, X., & Ferreira, L., G.** (2002). Overview of the
19
20 radiometric and biophysical performance of the MODIS vegetation indices. *Remote Sensing of*
21
22 *Environment*, 83, 195-213.

23
24
25 **IPCC.** (2007). Contribution of working groups I, II and III to the fourth assessment report of the
26
27 intergovernmental panel on climate change. Core writing team, Pachauri, R. K. & Reisinger, A.
28
29 (Eds.). Geneva, Switzerland, 104 pages.

30
31
32 **Junk, W.J., Bayley, P.B., Sparks, R.E.** (1989). The flood pulse concept in river-floodplain
33
34 systems. *Can. Spe. Publ. Fish. Aquat. Sci.* 106: 110-127.

35
36
37 **Junk, J.W., Fernandez Piedade, M.T., Schöngart, J., Cohn-Haft, M., Adeney, J.M., Wittmann,**
38
39 **F.** (2011). A classification of major Naturally-Occuring Amazonian Lowland Wetlands. *Wetlands*,
40
41 31, 623-640.

42
43
44 **Keddy, P. A., Fraser, L. H., Solomeshch, A. I., Junk, W. J., Campbell, D. R., Arroyo, M. T. &**
45
46 **Alho, C. J.** (2009). Wet and wonderful: the world's largest wetlands are conservation priorities.
47
48 *BioScience* 59(1), 39-51.

49
50
51 **Laraque, A., Maziéoula, B.** (1995). **Banque de données hydrologiques des affluents du fleuve**
52
53 **Congo-Zaïre et informations physiographiques, rapport interne lab. HydrORSTOM,**
54
55 **Montpellier, 250 p**

56
57 **Lefsky, M.A., Keller, M., Pang, Y., De Camargo, P. B., & Hunter, M.O.** (2007). Revised method
58
59
60

1
2 for forest canopy height estimation from Geoscience Laser Altimeter System Waveforms, *Journal*
3 *of Applied Remote Sensing*, 1,1-18.

4
5
6 **Lepersonne J.** (1974). Carte géologique du Zaïre 1/2000000. Rep. Du Zaïre, commissariat d'état
7
8 aux mines, service géologique, Kinshasa.

9
10 **Léonard, J.** (1947): Contribution a l'étude des formations ripicoles arbustives et arborescentes de la
11
12 région d'Éala, C.R. Sem. Agr. Jangambi.

13
14 **Maltby, E.,** (1986). *Waterlogged wealth: why waste the world's wet places ?* , Russel Press,
15
16 Nottingham, 200 p.

17
18 **Maltby, E.** (1991). Wetland management goals : wise use and conservation. *Landscape and Urban*
19
20 *planning*, 20 (1-3), 9-18.

21
22 **Martinez, J.-M. & Le Toan, T.** (2007). Mapping of flood dynamics and spatial distribution of
23
24 vegetation in the Amazon floodplain using multitemporal SAR data *Remote Sensing of*
25
26 *Environment*, 108(3), 209-223.

27
28
29 **Misser F.** (2003). RD Congo: economy. In: *Africa South of the Sahara 2003*, 22nd edition. Europa
30
31 Publ. London 1360 p.

32
33 **Mitsch, W.J. & Gosselink, J.G.** (2007). *Wetlands* 4th ed., Wiley, Oxford, 600 p

34
35 **Moukolo, N., Laraque, A., Olivry, J. C. & Briquet, J. P.** (1993). Transport en solution et en
36
37 suspension par le fleuve Congo (Zaïre) et ses principaux affluents de la rive droite. *Hydrological*
38
39 *Science Journal*, 38(2), 133–145.

40
41
42 **Murdoch, P.S., Baron, J.S., Miller, T.L.** (2000). Potential effects of climate change on surface-
43
44 water quality in north america. *JAWRA Journal of the American Water Resources Association*,
45
46 36(2), pp,347–366.

47
48
49 **Neuenschwander, A.L., Urban, T.J., Gutierrez, R., Schutz, B.E.** (2008). Characterization of
50
51 ICESat/GLAS waveforms over terrestrial ecosystems: Implications for vegetation mapping, *Journal*
52
53 *of Geophysical Research*, N°113 (G02S03).

1
2
3
4
5
6
7
8
9
10
11
12
13
14
15
16
17
18
19
20
21
22
23
24
25
26
27
28
29
30
31
32
33
34
35
36
37
38
39
40
41
42
43
44
45
46
47
48
49
50
51
52
53
54
55
56
57
58
59
60

OECD. (1996). The knowledge-based economy. Organisation for economic co-operation and Development, Paris.

Parolin, P. (2009). Submerged in darkness: adaptations to prolonged submergence by woody species of the Amazonian floodplains. *Annals of Botany*, 103, 359-376.

Parolin, P., Waldhoff, D. & Zerm, M. (2010). Photochemical capacity after submersion in darkness: how Amazonian floodplain trees cope with extreme flooding. *Aquatic Botany*, 93: 83-88.

Parolin, P. & Wittmann, F. (2010). Struggle in the flood: tree responses to flooding stress in four tropical floodplain systems. *AoB PLANTS* 2010: plq003, doi:10.1093/aobpla/plq003.

Peixoto, J. M. A., Nelson, B. W. & Wittmann, F. (2009). Spatial and temporal dynamics of river channel migration and vegetation in central Amazonian white-water floodplains by remote-sensing techniques. *Remote Sensing of Environment*, 113, 2258-2266.

Pennec, A., Gond, V. & Sabatier, D. (2011). Characterization of tropical forests phenology in French Guiana using MODIS time-series, *Remote Sensing Letters*, 2(4), 337-345.

RAMSAR. (1971). Convention relative aux zones humides d'importance internationale, particulièrement comme habitats des oiseaux d'eau. United Nations n° 14 583.

Robert M. (1946). Le Congo physique. Comité Spécial du Katanga, 3rd Ed. Vaillant-Carmanne, Liège, 449 p
Moukolo N. Laraque A., Olivry J.-C. & Bricquet J.-P. 1993: Transport en solution et en suspension par le fleuve Congo (Zaïre) et ses principaux affluents de la rive droite. *Hydrological Sciences -Journal- des Sciences Hydrologiques*, 38(2,4), 133-145.

Rosenqvist, A., Forsberg, B. R., Pimentel, T. P., Rauste, Y. A., & Richey, J. E. (1999). The use of spaceborne radar data for inundation modelling and subsequent estimations of trace gas emissions in tropical wetland areas. In IRD (Ed.), Proceedings of the Hydrological and Geochemical Processes in Large Scale River Basins Conference. Manaus, Brazil.

Scarano, F.R., Ribeiro, K.T., De Moraes, L.F.D., De Lima, H.C. (1997). Plant establishment on flooded and unflooded patches of a freshwater swamp forest in Southeastern Brazil. *Journal of tropical ecology*, 13(6), 793-803.

1
2
3
4
5
6
7
8
9
Scarano, F.R., (1998). A comparison of dispersal germination and establishment of woody plants subjected to distinct flooding regimes in Brazilian flood-prone forests and estuarine vegetation, *Ecophysiological strategies of xerophytic and amphibious plants in the neotropics. Series Oecologia Brasiliensis*, 4, 177-193.

10
11
12
13
14
15
16
Schlüter, U.-B., Furch, B. & Joly, C. A. (1993). Physiological and anatomical adaptations by young *Astrocaryum jauari* Mart. (Arecaceae) in periodically inundated biotopes of Central Amazonia. *Biotropica*, 25, 384–396.

17
18
19
20
21
22
23
Schöngart, J., Piedade, M. T. F., Ludwighausen, S., Horna, V. & Worbes, M. (2002). Phenology and stem-growth periodicity of tree species in Amazonian floodplain forests. *Journal of Tropical Ecology*, 18, 581-597.

24
25
Shahin M. (2002). Hydrology and water resources of Africa. Springer Verlag, 659 p.

26
27
28
29
30
31
32
Thiel, C.J., Thiel, C., Schmullius, C.C. (2009). Operational Large-Area Forest Monitoring in Siberia Using ALOS PALSAR Summer Intensities and Winter Coherence, *IEEE Transaction on Geoscience and remote Sensing*, 47, 3993-4000.

33
34
35
36
Tibshirani, R., Walter, G., & Hastie, T. (2001). Estimating the number of clusters in a dataset via the gap statistic, *Journal of Royal Statistic Society B.*, 63, 411-423.

37
38
Thorndike, R., L. (1953). "Who Belong in the Family?". *Psychometrika*, 18.

39
40
41
42
43
Turton A. & Ashton P. (2004). Southern african water cooperation – lessons from the Okavango basin. CSIR-environmentek, Pretoria 24 slides.

44
45
46
47
48
49
50
Ulaby, F.T., Moore,R.K., & Fung, A.K. (1982). Microwave Remote Sensing, Active and Passive, 2, Radar Remote Sensing and Surface Scattering and Emission Theory. Addison-Wesley, advanced book program, Massachussetts, 609 pages.

51
52
53
54
55
56
57
58
59
60
Vancutsem, C., Pekel, J-F., Evrard, C., Malaisse, F., Defourny, P. (2009). Mapping and characterizing the vegetation types of the Democratic Republic of Congo using SPOT VEGETATION time series. *International Journal of Applied Earth Observation and Geoinformation*, 11, 62-76.

1 **Wang, Y., Hess, L. L., Filoso, S. & Melack, J. M.** (1995). Understanding the radar backscattering
2 from flooded and non-flooded Amazonian forests: Results from canopy backscatter modeling.
3
4 *Remote Sensing of Environment*, 54, 324-332.
5
6

7
8 **Wittman, F., Anhuf, D., Funk, W.F.** (2002). Tree species distribution and community structure of
9 central Amazonian varzea forests by remote sensing techniques. *Journal of Tropical Ecology*, 18,
10
11 805-820.
12
13

14 **Wright, S. J. & van Schaik, C. P.** (1994). Light and the phenology of tropical trees. *American*
15
16 *Naturalist*, 143(1), 192-199.
17

18 **Yayer J.** (1951). Caractéristiques hydrographiques de l'Oubangui. Min. Colonies Bruxelles, Comité
19
20 Hydrographique Congolais, 1(3), 30 p.
21
22

23 **Zwally, H.J., R. Schutz, C. Bentley, J. Bufton, T. Herring, J. Minster, J. Spinhirne, & R.**
24
25 **Thomas.** (2003). Updated current year. *GLAS/ICESat L2 Global Land Surface Altimetry Data*
26
27 *V018*, 15 October to 18 November 2003. Boulder, CO: National Snow and Ice Data Center. Digital
28
29 media.
30
31
32
33
34
35
36
37
38
39
40
41
42
43
44
45
46
47
48
49
50
51
52
53
54
55
56
57
58
59
60

Figures caption and Table

Figures

Figure 1. Location of the 'Cuvette Centrale' within the Congo River basin (Africa).

Figure 2. Figure 2. The average rainfall (mm), evapotranspiration (mm), and average monthly components of water budget in Mbandaka (m), (sources: FAO, 2000; Devroey, 1957).

Figure 3. The Thornlike index value vs. the number of clusters for unsupervised classification of the EVI index.

Figure 4. A map of the unsupervised classification using the EVI average year. The labeling takes into account the Evrard and Junk typology, the PALSAR, the GLAS and the EVI information. The map corresponds to the EVI unsupervised classification with a masked inundated landscape (Bwangoy *et al.*, 2010).

Figure 5. Repartition percentage of each EVI class in each IGN class; the surface area examined corresponds to approximately to 50,000 km². IGN-1 corresponds to forests subjected to seasonal flood pulse, localised along river, IGN-2 corresponds to forests subjected to relatively stable water level, IGN-3 corresponds to forests subjected to relatively stable water level and IGN-4 corresponds to non flooded forests (IGN, 1960).

Figure 6. Annual variation of the EVI index for each forest class.

Figure 7. The Thornlike index vs. the number of clusters for the unsupervised classification of the PALSAR images.

Figure 8. Annual variation of the mean backscattering coefficient and standard deviation for each PALSAR-derived class.

Figure 9. A map of the unsupervised classification results of 6 PALSAR products.

Figure 10. Forested wetland photographs from field

1
2
3
4
5
6
7
8
9
10
11
12
13
14
15
16
17
18
19
20
21
22
23
24
25
26
27
28
29
30
31
32
33
34
35
36
37
38
39
40
41
42
43
44
45
46
47
48
49
50
51
52
53
54
55
56
57
58
59
60

Figure 11. The relationship between photosynthetic activity and environmental parameters (rainfall in mm, Oubangui and Congo flooding in $\text{m}^3 \cdot \text{s}^{-1}$ and light intensity in $\text{cal g/cm}^2/\text{day}$) at two stations located in the Cuvette Centrale: Eala (18.28°E ; 0.0°) and Lukolela (17.18°E ; 1.08°S).

Table

Table 1. EVI class structure characteristics documented with ICESAT-GLAS data.

For Review Only

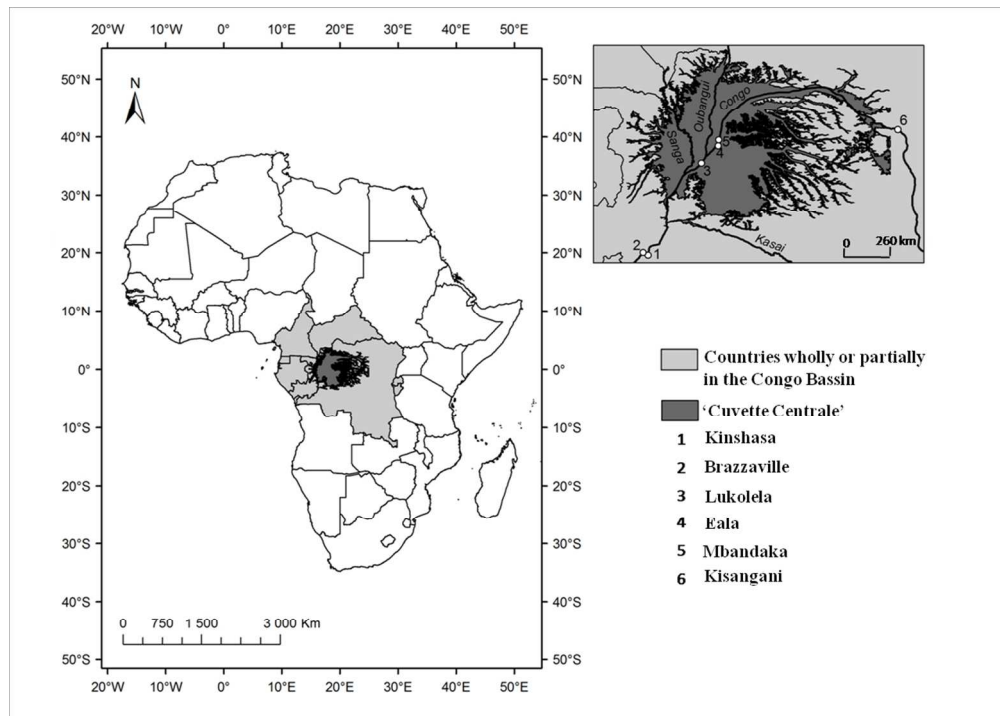


Figure 1. Location of the 'Cuvette Centrale' within the Congo River basin (Africa).

1
2
3
4
5
6
7
8
9
10
11
12
13
14
15
16
17
18
19
20
21
22
23
24
25
26
27
28
29
30
31
32
33
34
35
36
37
38
39
40
41
42
43
44
45
46
47
48
49
50
51
52
53
54
55
56
57
58
59
60

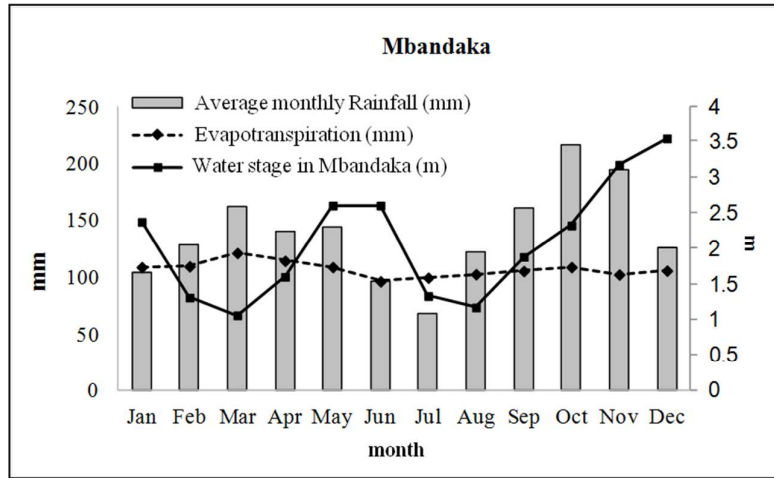


Figure 2. The average rainfall (mm), evapotranspiration (mm), and average monthly components of water budget in Mbandaka (m), (sources: FAO, 2000; Devroey, 1957).

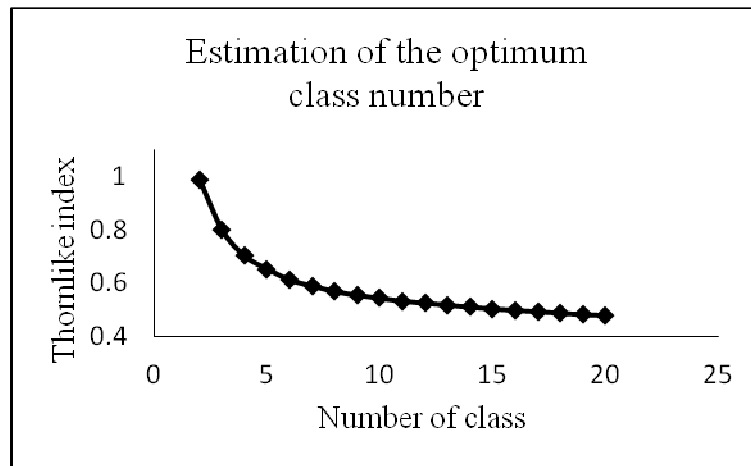


Figure 3. The Thomlike index value vs. the number of clusters for unsupervised classification of the EVI index.

For Review Only

1
2
3
4
5
6
7
8
9
10
11
12
13
14
15
16
17
18
19
20
21
22
23
24
25
26
27
28
29
30
31
32
33
34
35
36
37
38
39
40
41
42
43
44
45
46
47
48
49
50
51
52
53
54
55
56
57
58
59
60

1
2
3
4
5
6
7
8
9
10
11
12
13
14
15
16
17
18
19
20
21
22
23
24
25
26
27
28
29
30
31
32
33
34
35
36
37
38
39
40
41
42
43
44
45
46
47
48
49
50
51
52
53
54
55
56
57
58
59
60

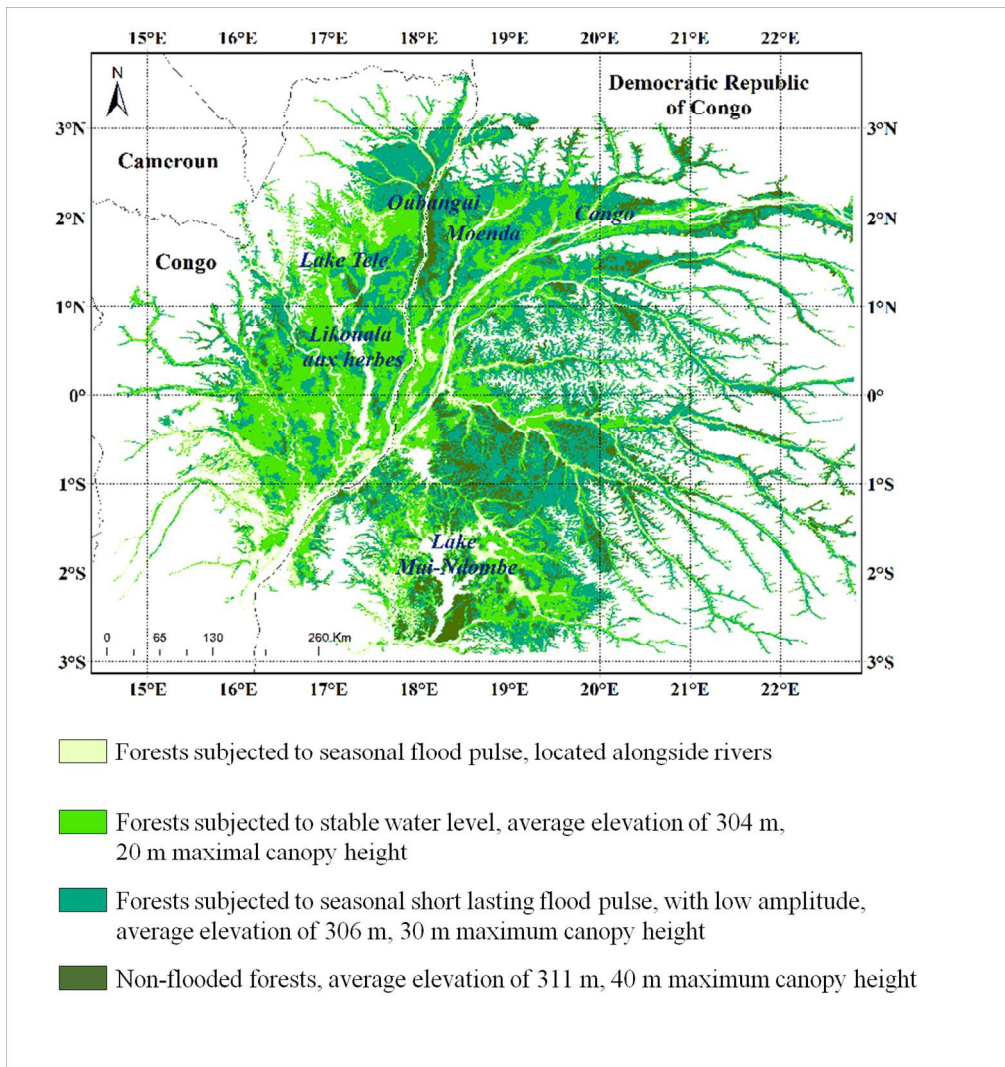


Figure 4. A map of the unsupervised classification using the EVI average year. The labeling takes into account the Evrard and Junk typology, the PALSAR, the GLAS and the EVI information. The map corresponds to the EVI unsupervised classification with a masked inundated landscape (Bwangoy et al., 2010).

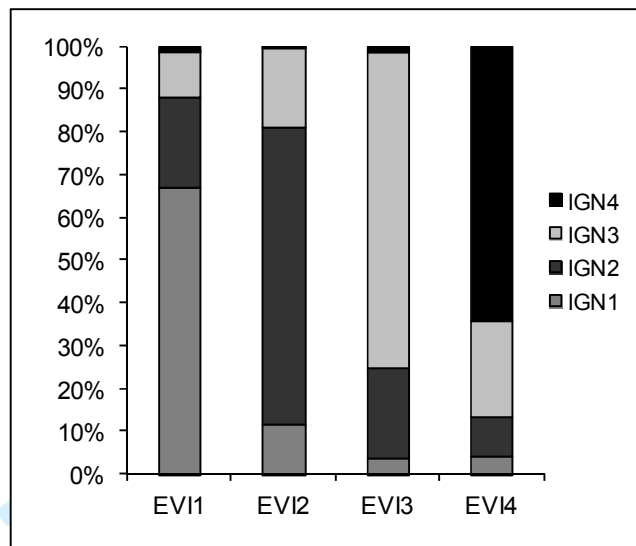


Figure 5. Repartition percentage of each EVI class in each IGN class; the surface area examined corresponds to approximately to 50,000 km². IGN-1 corresponds to forests subjected to seasonal flood pulse, localised along river, IGN-2 corresponds to forests subjected to relatively stable water level, IGN-3 corresponds to forests subjected to relatively stable water level and IGN-4 corresponds to non flooded forests (IGN, 1960).

1
2
3
4
5
6
7
8
9
10
11
12
13
14
15
16
17
18
19
20
21
22
23
24
25
26
27
28
29
30
31
32
33
34
35
36
37
38
39
40
41
42
43
44
45
46
47
48
49
50
51
52
53
54
55
56
57
58
59
60

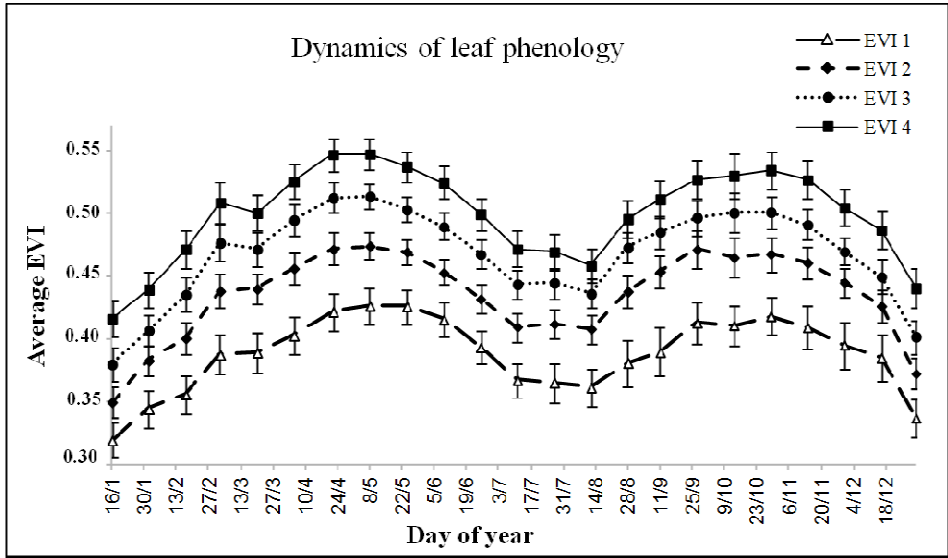
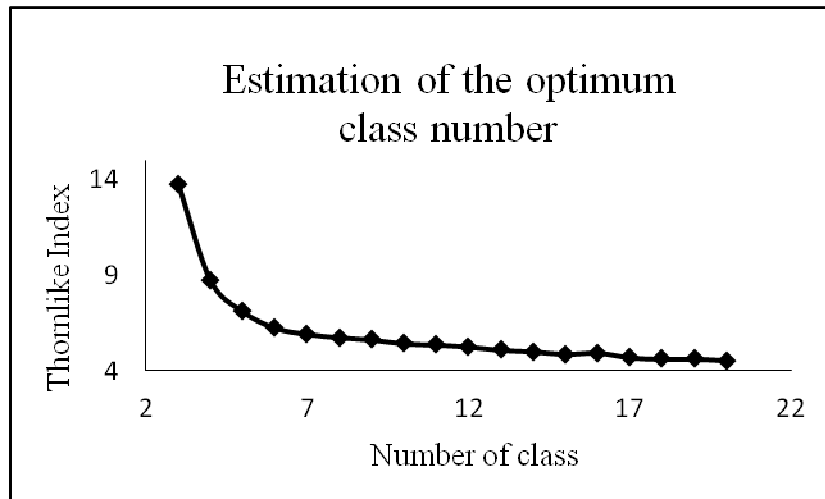


Figure 6. Annual variations of average EVI (and associated standard deviation) for each forest class

Review Only



20
21
22
23
24
25
26
27
28
29
30
31
32
33
34
35
36
37
38
39
40
41
42
43
44
45
46
47
48
49
50
51
52
53
54
55
56
57
58
59
60

Figure 7. The Thornlike index vs. the number of clusters for the unsupervised classification of the PALSAR images.

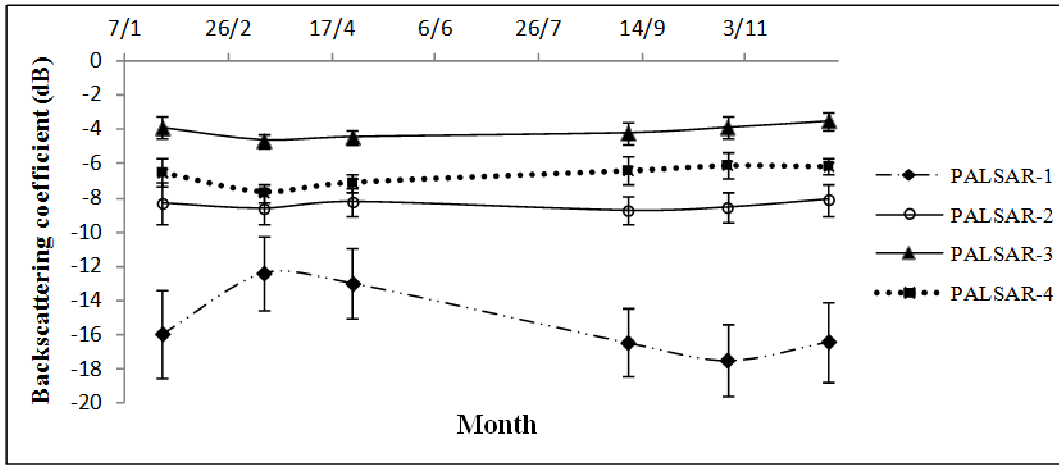


Figure 8. Annual variation of the mean backscattering coefficient and standard deviation for each PALSAR-derived class.

For Review Only

1
2
3
4
5
6
7
8
9
10
11
12
13
14
15
16
17
18
19
20
21
22
23
24
25
26
27
28
29
30
31
32
33
34
35
36
37
38
39
40
41
42
43
44
45
46
47
48
49
50
51
52
53
54
55
56
57
58
59
60

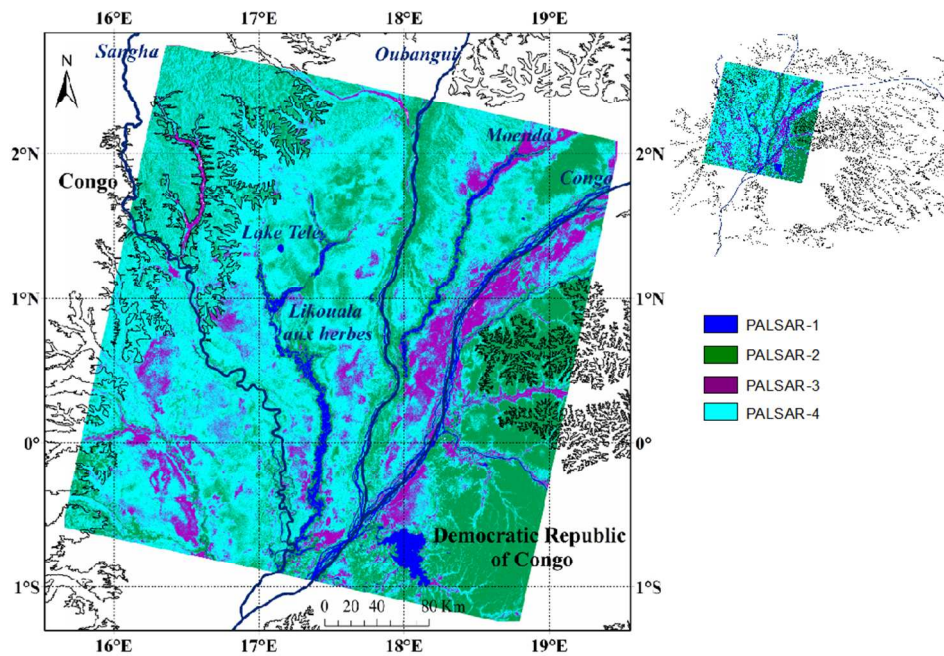


Figure 9. A map of the unsupervised classification results of 6 PALSAR products.

View Only

1
2
3
4
5
6
7
8
9
10
11
12
13
14
15
16
17
18
19
20
21
22
23
24
25
26
27
28
29
30
31
32
33
34
35
36
37
38
39
40
41
42
43
44
45
46
47
48
49
50
51
52
53
54
55
56
57
58
59
60

1
2
3
4
5
6
7
8
9
10
11
12
13
14
15
16
17
18
19
20
21
22
23
24
25
26
27
28
29
30
31
32
33
34
35
36
37
38
39
40
41
42
43
44
45
46
47
48
49
50
51
52
53
54
55
56
57
58
59
60





Class	Field Photographys
EVI 1 : forests subjected to seasonal flood pulse, located alongside rivers	 <p>Doumenge, C.</p>
EVI 2 : forests subjected to stable water level	 <p>Forni, E.</p>
EVI 3 : forests subjected to seasonal short lasting flood pulse, with low amplitude	 <p>Forni, E.</p>
EVI 4 : non-flooded forests	 <p>Gond, V.</p>

Figure 10. Forested wetland photographs from field

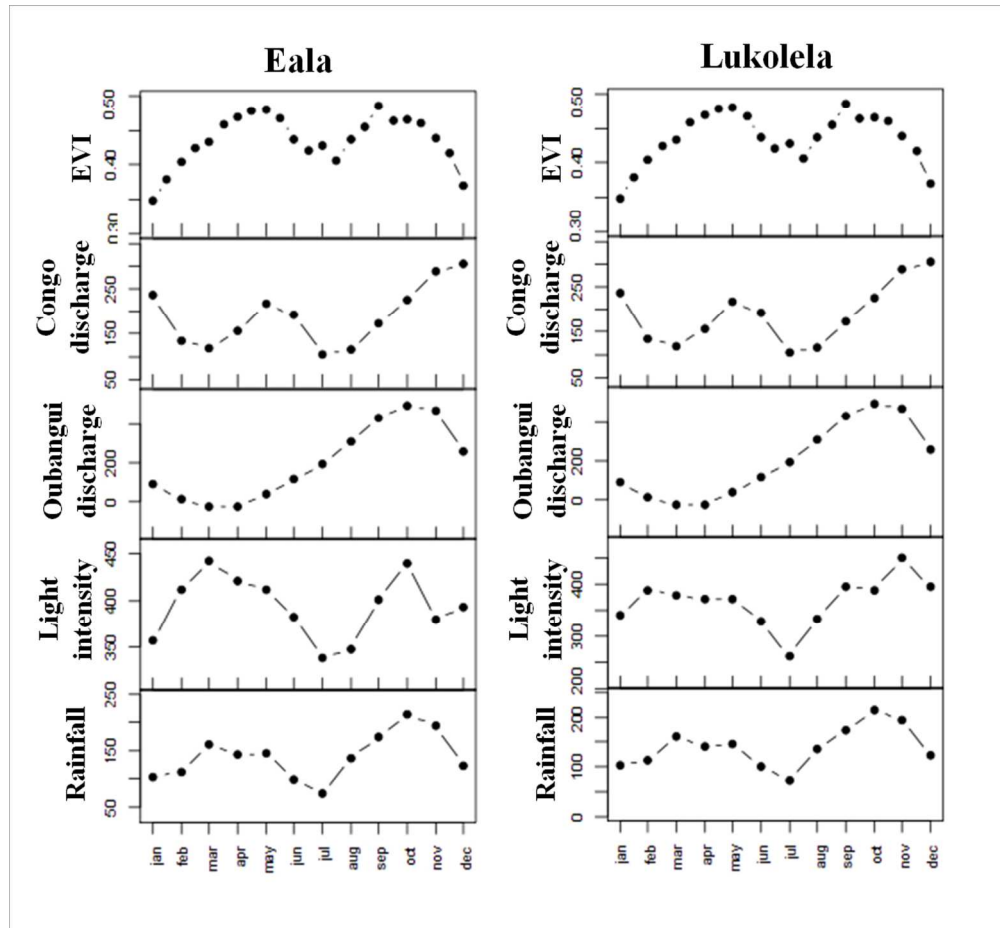


Figure 11. The relationship between photosynthetic activity and environmental parameters (rainfall in mm, Oubangui and Congo flooding in m³.s⁻¹ and light intensity in cal g/cm²/day) at two stations located in the Cuvette Centrale: Eala (18.28°E; 0.0°) and Lukolela (17.18°E; 1.08°S).

1
2
3
4
5
6
7
8
9
10
11
12
13
14
15
16
17
18
19
20
21
22
23
24
25
26
27
28
29
30
31
32
33
34
35
36
37
38
39
40
41
42
43
44
45
46
47
48
49
50
51
52
53
54
55
56
57
58
59
60

Class	Surface (km ²)	Average elevation (m)	Canopy maximum Height (m)	
			<i>Means</i>	<i>Std</i>
EVI-1	24 000	No Data	No Data	No Data
EVI-2	85 000	304	20	4.04
EVI-3	121 000	306	30	4.8
EVI-4	56 000	311	41	3.7

Table 1. EVI class structure characteristics documented with ICESAT-GLAS data.

For Review Only